



Research Article

Hydrothermal analysis of archimedean spiral single and dual channel heat sink for CPU cooling

Hala M. RASHAD¹, Younis M. NAJIM², Hatem H. ISMAEEL¹

¹Department of Energy Engineering, Duhok Polytechnic University, Duhok, 1006, Iraq

²Department of Mechanical Engineering, University of Mosul, Mosul, 41002, Iraq

ARTICLE INFO

Article history

Received: 05 June 2022

Accepted: 20 November 2022

Keywords:

Heat Sink; CPU Liquid Cooling;
Conjugate Heat Transfer;
Hydrothermal Performance;
Computational Fluid Dynamics

ABSTRACT

Engineering modeling and simulation represent a predominantly design tool in the modern manufacturing industry in which the actual system is reproduced using a mathematical and scientific model. This requires CPUs with higher computational capacities. However, increasing the computational capacities of CPU and GPU imposes challenges in the cooling process due to space limitations. CPU liquid cooling system has attracted more interest as an efficient heat dissipation tool. This work presents computational modeling of the conjugate heat and flow for the CPU liquid heat sink cooling. An Archimedean spiral channel is grooved into the cold plate of the heat sink. Single and dual channel passes are used in this work. The outer diameter of the cold plate is 105 mm and the channel depth is 5 mm for both single and dual-channel configurations. The conjugate heat sink model was constructed to have four different domains: CPU (alumina), glue layer (ethoxy), cold plate (copper), and liquid coolant (water). To incorporate the effect of turbulence, the flow rate varied to cover a range of Reynolds number from 3000 up to 15000 at a constant inlet temperature of 25 °C. The used turbulence model was the Shear Stress Transport (k- ω) to better capture the viscous, high-frequency flow fluctuation in the near-wall region. The bottom surface of the CPU is subjected to 450 W of heat energy. The results showed that the channel configuration and Reynolds number have a decisive impact on controlling the CPU temperature. The CPU temperature decrease as Reynolds number increases, however, the pressure drop increases at an exponential rate. These findings are supported by Darcy–Weisbach equation for internal flow in which the pressure drop depends on the square of the average fluid velocity and it was noticed that the pressure drop in the dual channel was three times higher than that in the single channel. The hydrothermal performance of the Archimedean spiral channel rapidly decreased with Reynolds number and the single-channel had a slightly better performance compared with the dual-channel.

Cite this article as: Rashad HM, Najim YM, Ismaeel HH. Hydrothermal analysis of archimedean spiral single and dual channel heat sink for cpu cooling. J Ther Eng 2024;10(1):50–61.

*Corresponding author.

*E-mail address: address:halamamun80@gmail.com

*This paper was recommended for publication in revised form
by Ahmet Selim Dalkılıç*



INTRODUCTION

The recent developments in computational hardware and algorithms have advanced the electronic devices' capabilities to be used widely in engineering modeling, industrial applications, communication systems, high-performance computers, satellites, aircraft, space shuttles, and many other applications. To meet the requirements of speed and accuracy, the new generations of CPU and GPU are characterized by high computing power and compactness which, however, intensify the heat emission. Conventional air cooling is no longer able to dissipate the heat and keep the temperature of CPU and GPU within safe values, therefore, the cooling process becomes a challenging problem [1]. As a consequence, CPU liquid cooling received considerable attention in recent years to protect CPUs from overheating, malfunctioning, or permanent damage [2–6].

It has been shown that CPU liquid cooling can dissipate 70 to 78% of the heat released by electronic elements [7]. Several technologies of thermal management have been reported in the literature to manage the increased heat flux generated by CPU using liquid cooling [8]. For example, liquid-cooled micro/mini channels were investigated first by Tuckerman and Pease [9] in 1981. They used a microchannel heat sink with water as a coolant to remove high heat flux of 790 W/m². The pressure drop was 210 kPa and the substrate temperature rise of 71 °C. Chang et al. [10] employed microchannel heat sink and heat rejector using deionized water as a coolant to dissipate the heat flux generated by the CPU of personal computers. The cold plate consisted of 38 microchannels with a vertical impinged inlet and two horizontal outlets. Furthermore, Abdulnabi et al. [11] conducted a numerical and experimental investigation on the hydraulic and thermal performance of four different serpentine channel configurations to cool off electronic devices. Three configurations were used with two inlets and two outlets while the other one has one inlet and one outlet. Liquid water with a flow rate of 0.01 kg/s was used as a coolant. The flow was laminar, the heat flux was 400 W/m², and the dimensions of the blocks were 150 mm × 100 mm × 10 mm. The results showed that the configurations with two inlets and outlets are showing better performance than the conventional one with one inlet and one outlet.

Other techniques such as the one reported by Sahu et al. [12] have been investigated. A hybrid cooling system was introduced by combining two cooling techniques; solid-state and microfluidic to cool off a hot spot under a heat flux of 250 W/m². The effect of hotspot size and the ambient temperature was taken into consideration. Moreover, film evaporation with an enhanced fluid delivery system (FEEDS) was used for cooling electronic devices to examine the heat transfer coefficient and the pressure drop reported by Mandel et al. [13]. Two chips have been tested in two ways each one with a heat flux of 1kW/cm². The first one was made of Si and tested in a press-fit FEEDS while the second one was tested in a bonded FEEDS and made

of SiC. The experiment was performed based on different mass flow rates ranging from 3 to 12 g/s. The results showed that the vapor quality and the coefficient of performance of the first chip were 45% and 1400, respectively. Whereas the second one showed vapor quality of 85% and heat densities approaching 490 W/cm³. It is found that the working fluid has a considerable effect on the cooling process, therefore, different types of working fluids such as nanofluid, ethylene glycol, and other coolants can be found in the literature for this purpose. Sohel et al [14] studied the thermophysical properties and the heat transfer performance of three different nanofluids (Al₂O₃–Water, TiO₂–Water, and CuO–Water nanofluids) in a circular microchannel heat sink which was made of a 10 mm×10 mm×4 mm block with a circular channel of 400 μm. The flow was assumed to be steady, laminar, and incompressible with constant heat flux and inlet velocity of 1.5 m/s. It was found that the CuO–Water showed better performance than the other two fluids. Furthermore, different nano-fluids were also investigated such as Ferro-nanofluid, NiO–Water, and Fe₃O₄–Water [15–17].

Another type of working fluid is the phase change materials (PCM) reported by Gaikwad et al. [18]. They experimentally investigated the potential of using a straight microchannel heat sink with phase change materials (PCMs) for CPU cooling as they compared the PCM (slurry) with water under various flow rates of 75 to 300 ml/min and two different aspect ratios of 2 and 3. They found out that the PCM is more effective than water as it's capable of maintaining the temperature of the CPU lower than the second case by using water as a coolant for the same pumping power and mass flow rate.

Moreover, to increase the heat transfer surface area and provide better flow mixing by interrupting the steady flow, different types of fin heat sinks are introduced in the literature for improving heat dissipation [19,20]. To achieve efficient cooling, several channel shapes and configurations have been investigated such as straight minichannels [21], convergent-divergent, sinusoidal wavy, zigzag [22], and serpentine [23]. It was concluded that the sinusoidal wavy microchannel heat sink achieves a better heat transfer rate with acceptable pressure drop compared with other channel configurations. Additionally, the spiral tube exhibited better heat transfer performance over the taper helical tube in heat exchanger application [24]. Several conclusions can be drawn from the literature survey: (1) the new generation of CPU and GPU generates more heat than the conventional air cooling systems can tackle the cooling process, (2) other coolant types can also enhance the cooling rate, (3) the channel shapes and configurations show a considerable effect on the heat removal process and are still an active area of research to achieve efficient cooling with minimal pumping power, (4) the previous literature indicates that there is a lack of work on CPU heat sink cooling using Archimedean spiral channel [25].

This work numerically investigates the conjugate heat transfer in a CPU heat sink using water as a coolant. The channel is designed using an Archimedean spiral curve with single and dual flow passes. The Reynolds number varies from 3000 to 15000 and the associated CPU temperature, thermo-hydraulic performance, and pressure drop are monitored for both single and dual-channel configurations.

NUMERICAL MODELLING

Archimedean spiral channel heat sinks are proposed here as a heat sink to remove the undesirable heat from the CPU. The spiral channels are constructed using the Archimedean curve which can be mathematically described by [26]:

$$x = A t \cos\left(\frac{t}{2\pi}\right) \tag{1}$$

$$y = A t \sin\left(\frac{t}{2\pi}\right) \tag{2}$$

Where x and y represent a set of points equivalent to the positions of a point moving away from the curve center. Parameter A is varied here to control the channel width while the parameter t is adjusted to extend the channel outer diameter up to 100 mm. Both single and dual spiral channels have a depth of 5 mm and 0.5 mm wall thickness. Detailed channel dimensions are presented in Table 1. The working fluid is allowed to enter both configurations at the

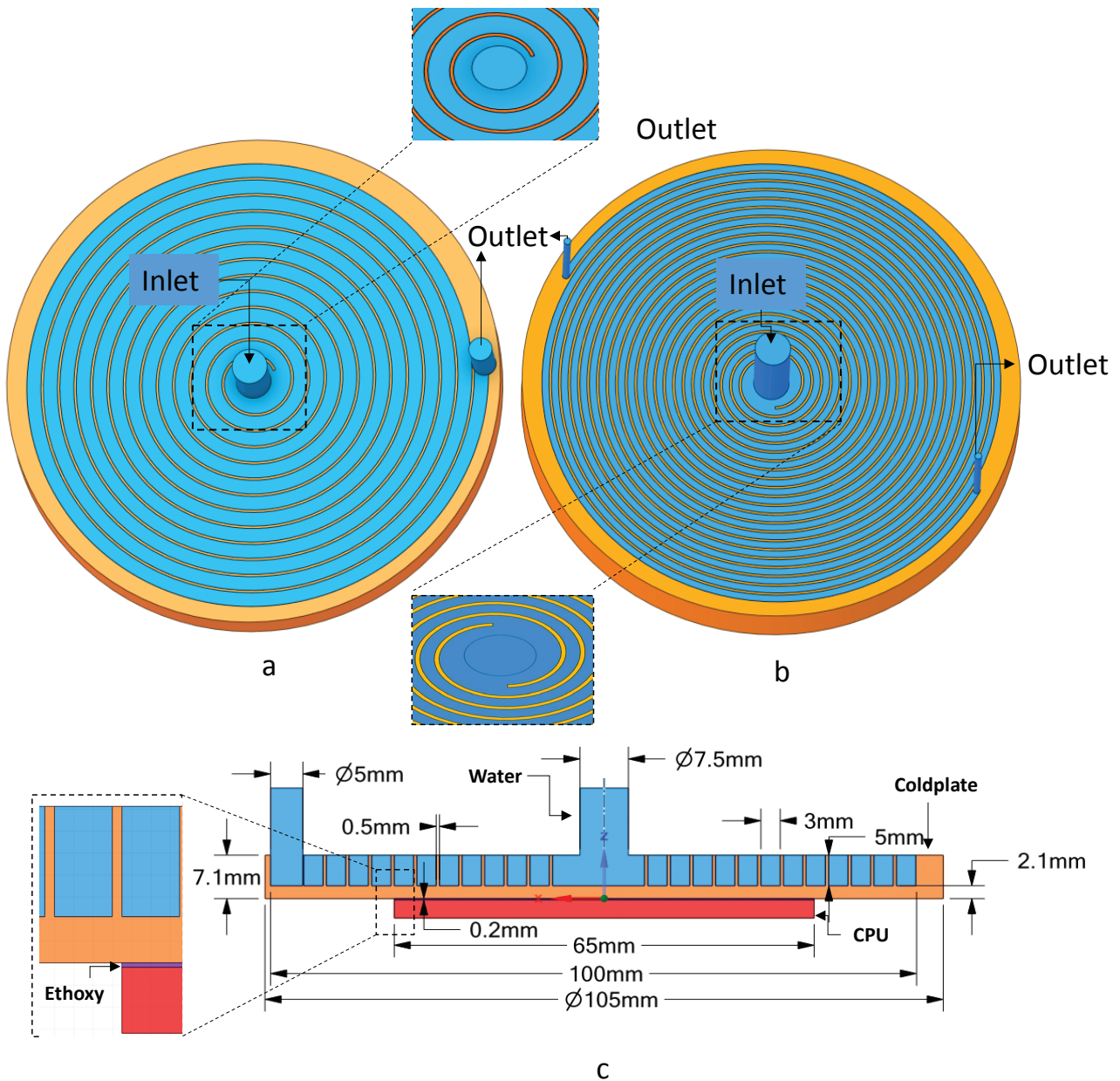


Figure 1. Archimedean Spiral channel heat sinks (a) Single-channel (b) Dual-channel (c) cross-section of single channel.

Table 1. Channel Dimensions

Channel	Single	Dual
W_{ch}	3 mm	1.5 mm
H_{ch}	5 mm	5 mm
δ_{wall}	0.5 mm	0.5 mm
D_h	3.75 mm	2.308 mm
Archimedean Curve		
Start (t)	8.5	8.5
End (t)	89.7597901	78.53981634
A	3.5	4
Y	49.99956058	49.0031507
X	0.209622066	9.934345548
Cold plate		
D	105mm	105 mm
H	7.1 mm	7.1 mm

center of the cold plate which facilitates higher heat removal as the heat intensifies at the center as shown in Figure 1-a and b. The heatsink was made of copper aiming for higher thermal conductivity and good machinability. The CPU is modeled as a rectangular plate with 65mm x 65mm x 3mm and made of alumina. The CPU sticks to the heatsink using an ethoxy thin (200 μ m) layer. The material properties of Water, Alumina, copper, and ethoxy are listed in Table 2.

Heat and Fluid Flow Governing Equations

The fluid flow inside the channel can be mathematically described using Reynolds Averaged Navier-Stokes equations (RANS). The RANS equations describe the fluid velocity, pressure, and temperature of a computational element. The RANS has a closure problem that needs to be addressed using turbulence models [28]. The flow conditions are assumed as single-phase, steady, constant density, incompressible, non-reacting flow. The Navier Stokes equation can be expressed in a vector form as[29]:

$$\frac{\partial \bar{u}_i}{\partial x_i} = 0 \tag{3}$$

$$\rho \frac{\partial \bar{u}_i}{\partial t} + \rho \bar{u}_k \frac{\partial \bar{u}_i}{\partial x_k} = -\frac{\partial p}{\partial x_i} + \frac{\partial}{\partial x_j} \mu \left(\frac{\partial \bar{u}_i}{\partial x_j} \right) + \frac{\partial R_{ij}}{\partial x_j} \tag{4}$$

It should be noted here that the transient term in the momentum equations is used by the solver to advance the iterations and not to account for transient evolution of the flow velocity and pressure. The momentum equation has a closure problem as the term ($R_{ij} = \rho u'_i u'_j$) is introduced by Reynolds average of the instantaneous momentum equation and is known as Reynolds stress tensor. The Reynolds stress tensor is modeled based on Boussinesq eddy-viscosity approximation such as [29]:

$$R_{ij} = \rho \overline{u'_i u'_j} = \mu_t \left(\frac{\partial \bar{u}_i}{\partial x_j} + \frac{\partial \bar{u}_j}{\partial x_i} \right) - \frac{2}{3} \rho k \delta_{ij} \tag{5}$$

The most common turbulence models used for eddy viscosity (ν_t) in channel flow are the k- ϵ and k- ω models. The k- ω model offers better treatment of the flow in the near-wall region which is characterized by viscous, high-frequency fluctuation flow. However, for mean flow near the channel centerline k- ϵ appears to be more accurate. In 1994, Menter [30,31] introduced the SST model which is a hybrid model that combines the advantages of the k- ϵ and k- ω model and produces more accurate results compared to the Direct Numerical Simulation (DNS) and the experimental results [19,32,33]. The SST model can be introduced as follows [30,31]:

$$\frac{\partial k}{\partial t} + \bar{u}_j \frac{\partial k}{\partial x_j} = \left(\frac{\partial \bar{u}_i}{\partial x_j} + \frac{\partial \bar{u}_j}{\partial x_i} \right) \frac{\partial \bar{u}_i}{\partial x_j} - \beta' \omega k + \frac{\partial}{\partial x_i} \left[(\nu + \sigma_k \nu_t) \frac{\partial k}{\partial x_i} \right] \tag{6}$$

$$\frac{\partial \omega}{\partial t} + \bar{u}_j \frac{\partial \omega}{\partial x_j} = \frac{\lambda}{\nu_t} \left(\frac{\partial \bar{u}_i}{\partial x_j} + \frac{\partial \bar{u}_j}{\partial x_i} \right) \frac{\partial \bar{u}_i}{\partial x_j} - \beta \omega^2 + \frac{\partial}{\partial x_i} \left[(\nu + \sigma_\omega \nu_t) \frac{\partial \omega}{\partial x_i} \right] + 2(1 - F_1) \frac{\sigma_{\omega 2}}{\omega} \frac{\partial k}{\partial x_i} \frac{\partial \omega}{\partial x_i} \tag{7}$$

$$\nu_t = \frac{a_1 k}{\max(a_1 \omega, \Omega F_2)} \tag{8}$$

The values of model parameters (β' , σ_k , λ , β , σ_ω , $\sigma_{\omega 2}$) are given in [30][31]. Since the flow is incompressible, the energy is solved iteratively as a transport equation after the continuity and momentum equations are converged. The energy equation for fluid can be expressed as [7]:

$$\rho \left(u_i \frac{\partial T_f}{\partial x_i} \right) = \frac{\mu}{Pr} \left(\frac{\partial^2 T_f}{\partial x_i^2} \right) \tag{9}$$

Table 2. Material properties [27]

Properties	Water	Copper	Ethoxy	Alumina
Density [Kg/m ³]	998.2	8978	2300	3900
Specific Heat [J/(Kg.K)]	4182	381	1460	900
Thermal Conductivity[W/(m.k)]	0.6	387.6	2.2	27
Viscosity [Kg/m.s]	0.001003	-----	-----	-----

For solid computational domains which include cold plate, CPU, and ethoxy layer, the conduction energy equation is used to model the heat transfer which can be reduced to:

$$k \left(\frac{\partial^2 T_s}{\partial x_i^2} \right) = 0 \quad (10)$$

The equations above are discretized using finite volume analysis and solved iteratively using available solver Ansys fluent to provide a temperature field for solid domains and pressure, velocity as well as temperature for liquid water domain.

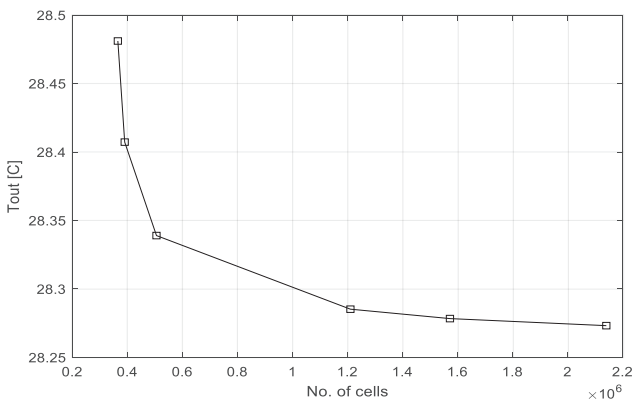


Figure 2. The effect of mesh size on the outlet temperature (Mesh independent study).

Grid Generation

It is an essential step for computation fluid dynamics to discretize the computational domain into small computational elements called cells (shown in Figure 3). This is because fundamental physical principles such as the first law of thermodynamics cannot be applied to a system (or computational domain) that does not satisfy thermal and mechanical equilibrium conditions. Since the temperature of the system varies significantly from inlet to outlet, and from CPU to cold plate, therefore, thermal equilibrium cannot be established. For this, the computational domain is divided into small cells of a size that is small enough to be considered a very small system with constant temperature, pressure, and other thermophysical properties. Hence the thermal equilibrium can be assumed with acceptable accuracy.

How small the cell size should be, is a key question in every CFD case under specific operating conditions. There is no direct method to determine the appropriate cell size for specific operating conditions. However, the mesh-independent study is a common scheme used to ensure that the mesh size is enough to capture the physics variation in the computational domain. This scheme is basically to start with a coarse mesh size and then gradually refine the mesh size while monitoring an output parameter that is sensitive enough to the mesh size such as water outlet temperature, see Figure 2. When the output parameter approaches a steady condition and no longer varies with the mesh size (or number of cells), we can assume that the corresponding mesh size is enough to capture the physics variations.

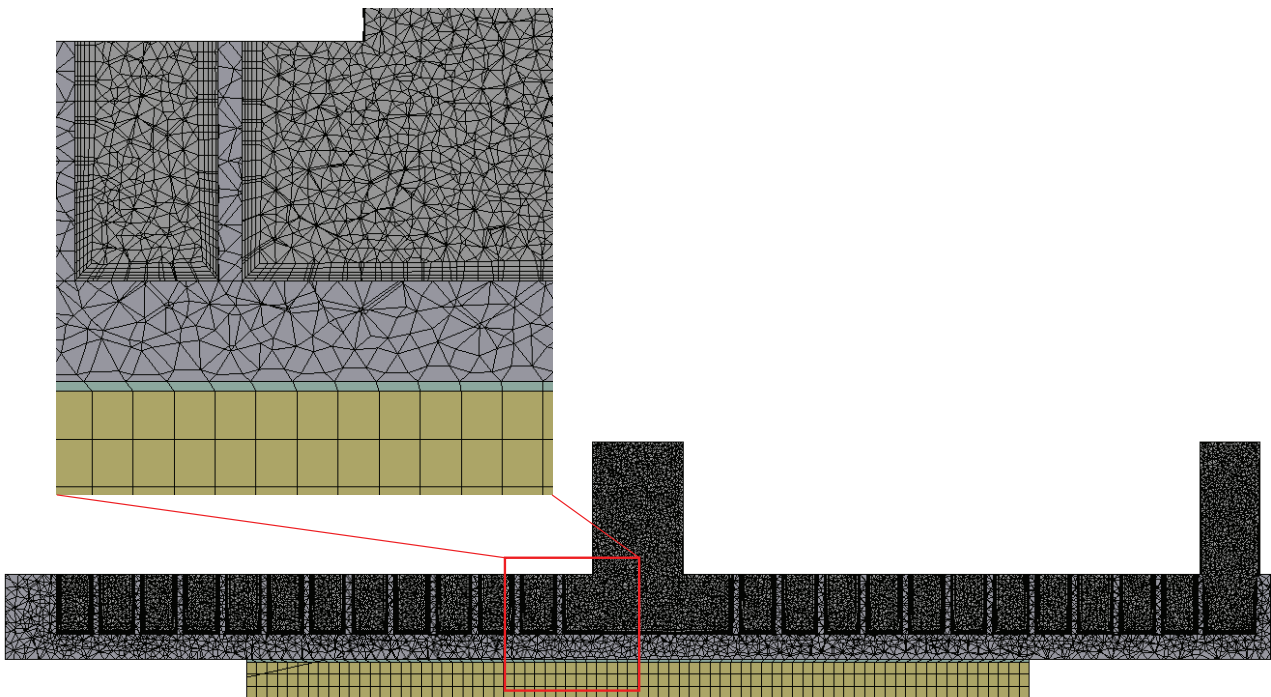


Figure 3. The grid structure of all domains.

In this study, the outlet temperature shows no significant variation beyond 2 million cells. However, the mesh of the fluid domain is further refined up to 5.8 million to capture the velocity profile in the spiral channel.

Boundary Conditions

The numerical solution of RANS is highly dependent on the boundary conditions which must be realistic to ensure the convergence of the iterative solver. In this work, the no-slip condition is applied to all domains' walls which means the flow velocity is brought to zero, ($u=v=w=0$). Since the flow is considered incompressible, the inlet flow velocity (V_{in}) and temperature ($T_{f,in}$) are specified. The inlet velocity is varied such that the Reynolds number is changed from 3000 to 15000 while the inlet temperature is kept unchanged at 25°C. The outlet pressure is assumed atmospheric ($P=0$ atm.). The fluid top surface and all external walls of the solid domains are considered adiabatic except for the CPU bottom surface which is subjected to a constant heat flux based on the dissipated power of 450 W.

Data Reduction

The hydrothermal performance of the single and dual spiral channel under specific flow conditions can be expressed by two factors: (1) the Nusselt number (Nu) which expresses the performance of the channel in heat transfer rate and (2) the required pumping power which is determined by Fanning friction factor (f). The two factors can be cast in one equation commonly known as the Performance Evaluation Criterion (PEC) as follows [34,35]:

$$PEC = \frac{(Nu/Nu_0)}{(f/f_0)^{1/3}} \quad (11)$$

Where Nu_0 , and f_0 represent the Nusselt Number and the fanning friction factor of the straight channel using (Dittus and Boelter) equation for Nusselt number ($Nu_0 = 0.023Re^{0.8} Pr^{0.4}$)[36] and Blasius equation for fanning friction factor [$f_0 = 0.079Re^{-0.25}$][37]. The Nu and f represent the Nusselt Number and the fanning friction factor of the single and dual channel respectively [38].

$$Nu = \frac{h_m D_h}{k_f} = \frac{\dot{m} c_p (T_{out} - T_{in})}{A_s (T_s - \frac{T_{out} + T_{in}}{2}) k_f} \quad (12)$$

Where D_h is the hydraulic diameter of the channel, k_f is the fluid's conductivity and h_m represent the average heat transfer coefficient which can be calculated by [27]:

$$h_m = \frac{q A_{cpu}}{A_s (T_s - T_m)} \quad (13)$$

Here, q is the heat flux subjected to the bottom of the CPU, A_{cpu} the surface area of the CPU, A_s and T_s are the area and the temperature of the interface between the fluid and

the cold plate, and T_m is the mean fluid temperature and can be simplified using:

$$T_m = \frac{T_{in} + T_{out}}{2} \quad (14)$$

We can get the fanning friction factor from the equation shown below [37]:

$$f = \frac{\Delta P D_h}{2 * \rho_f u_{in}^2 L} \quad (15)$$

Where ΔP is the pressure drop across the channel length L , u_{in} is the velocity inlet and ρ_f is the density of the working fluid.

RESULTS AND DISCUSSION

Validation

To validate the computational scheme used in this work, a comparison is conducted with other work reported by Jilte et al. [25]. The comparison model uses a liquid-cooled heat sink consisting of four channels with a depth of 3.5 mm and a width of 4 mm. The heat flux applied to the bottom surface was based on the dissipated power of 50 W and 70W. The fluid's outlet temperature T_{out} was determined at different flow rates of 60 to 180 ml/min. The highest difference is observed at lower flow rates namely 60-100 ml/min. However, it can be concluded from Figure 4 that the numerical results agree with the previous study, especially for higher flow rates.

Temperature Field

The temperature distribution over CPU, ethoxy layer, copper plate, and cooling liquid are shown in Figure 5.

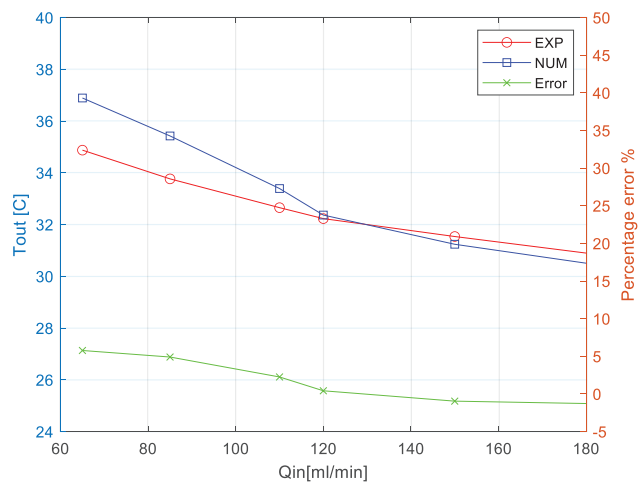


Figure 4. Variation of outlet temperature with the volume flow rate (Validation Results).

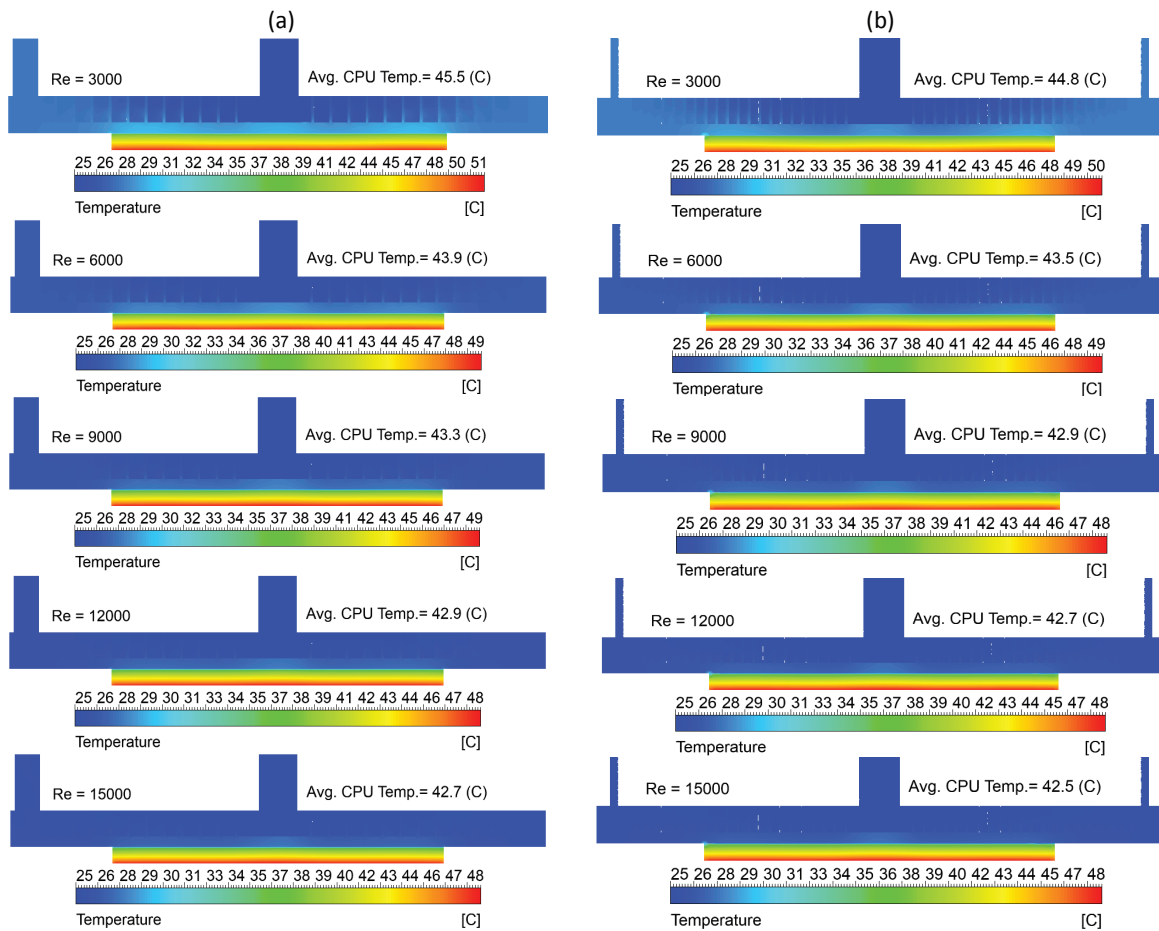


Figure 5. Temperature contours of (a) Single-channel and (b) Dual-channel.

The CFD analysis shows that the maximum temperature resides in the CPU since the heat flux is imposed on the bottom surface of the CPU. Therefore, the temperature variation is completely controlled by the thermal resistance of the individual computational domains. Evidence, for example, the copper plate which has higher thermal conductivity (lower thermal resistance) exhibits less temperature gradient compared with the CPU which has lower thermal conductivity. The results show that the temperature difference between the inlet and outlet of the water decreases as Reynolds number increases. It is found that the average temperature developed within the CPU decreases with Reynolds according to $T_{avg}^{single} = 45.96 + \frac{4793}{Re^{0.886}}$ and $T_{avg}^{dual} = 45.97 + \frac{8571}{Re^{0.980}}$ in °C for single and dual-channel, respectively. This shows that the channel configuration and Reynolds number have a decisive impact on controlling the CPU temperature. Figure 6 shows that the maximum and minimum differences between single and dual channels are 0.62°C at Re=3000 and 0.24°C at Re=15000 for CPU maximum temperature. The CFD temperature field contours uncover an important factor that may be attributed to the

enhancement of cooling. Since the channel wall is made of copper with lower thermal resistance, the temperature of the channel walls is higher than the bulk fluid temperature. Therefore, the channel walls can serve as fins immersed in water. Therefore, the dual channel offers more channel walls and hence a larger heat transfer surface area between (cold) fluid and (hot) solid walls.

The variation of CPU average and maximum temperatures with Reynolds number for both single and dual channels is illustrated in Figure 6. The CPU temperature exhibits a nonlinear rapid drop with the Reynolds number. The CPU temperature decreases dramatically for low Reynolds numbers (3000-8000) while the rate of change of CPU temperature decreases for higher Reynolds numbers.

Nusselt Number

The variation of the average Nusselt number for single and dual spiral channels with Reynolds number is shown in Figure 7. It shows that the difference between the single and dual spiral channels is marginal and slightly increases with Reynolds number. The dual spiral channel shows better heat transfer characteristics than the single channel. The maximum and minimum differences between the average

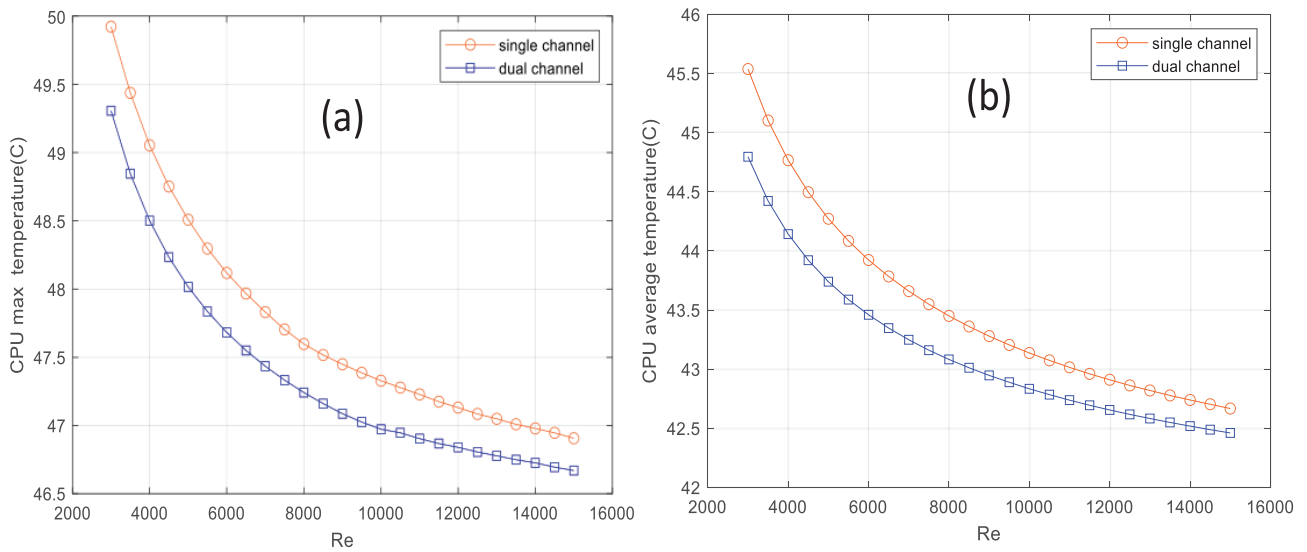


Figure 6. Variation of CPU (a) maximum temperature and (b) average temperature, with Reynolds number for both single and dual channels.

Nusselts number of dual and single are 5.16 at Re=15000 and 0.92 at Re=3000, respectively. Both single and dual spiral channels, however, develop significant enhancement in average Nusselt number compared with the straight channel. The results concluded that the Nusselt number increases by 52% for the dual spiral channel at Re=3000 and 55% at Re=15000 relative to the straight channel. The average Nusselt correlate with the Reynolds numbers according to $Nu=0.0328 Re^{0.85} Pr^{0.4}$ for single-channel and $Nu=0.335 Re^{0.85} Pr^{0.4}$ for dual-channel with a coefficient of determination (R-squared) of 0.9999 for both single and dual-channels. This is compared with the well-known Dittus-Boelter correlation ($Nu=0.023 Re^{0.8} Pr^{0.4}$) that is used

for straight-channel. The Prandtl number is determined at the average water temperature.

Pressure Drop

For laminar flow, the pressure drop is independent of the surface roughness, it increases with the equivalent channel length and fluid viscosity and decreases with the square of the channel hydraulic diameter. When the flow is turbulent, the surface roughness affects the pressure loss along with channel hydraulic diameter and length, fluid density, and average velocity. However, the flow in the spiral channel develops a non-symmetrical velocity profile, see Figure 9. Therefore, the theory based on simple channel flow may fail to predict the hydrothermal characteristics of the flow in the spiral channels. The pressure drop is a key parameter to estimate the required pumping power to determine the hydrothermal performance of the channel heat sink. Figure 8(b) shows that the spiral dual and single channels develop a maximum pressure drop of about 4000 kPa and 1000 kPa at Reynolds number 15000. At Re=3000, the Dual and single channels develop pressure drop of 211 and 75 kPa. It is found that the pressure drop increases at an exponential rate with Reynolds number according to $\Delta P_s = 0.05494Re^{1.755}$ and $\Delta P_d = 0.06803Re^{1.86}$ in Pa for single and dual channels, respectively. These findings are confirmed by Darcy-Weisbach equation for internal flow in which the pressure drop depends on the square of the average fluid velocity. Since the channel hydraulic diameter of the Dual-channel configuration is smaller than the single channel's one with the same velocity, the rate at which pressure drop increases in the Dual-channel with Reynolds number is much higher than that in the Single-channel.

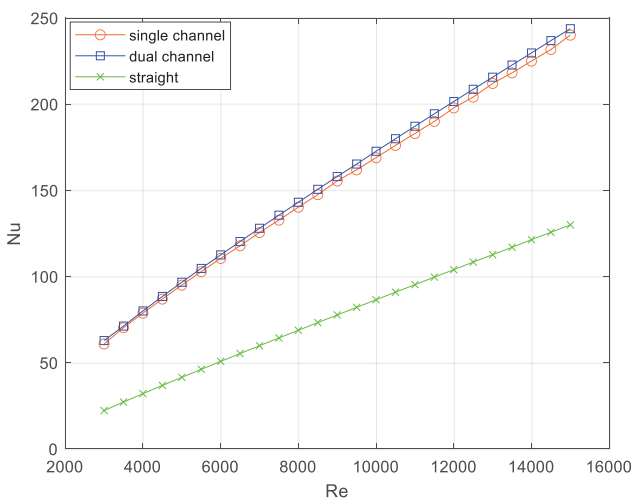


Figure 7. Variation of Nusselt number with Reynolds number for single, dual, and straight channels.

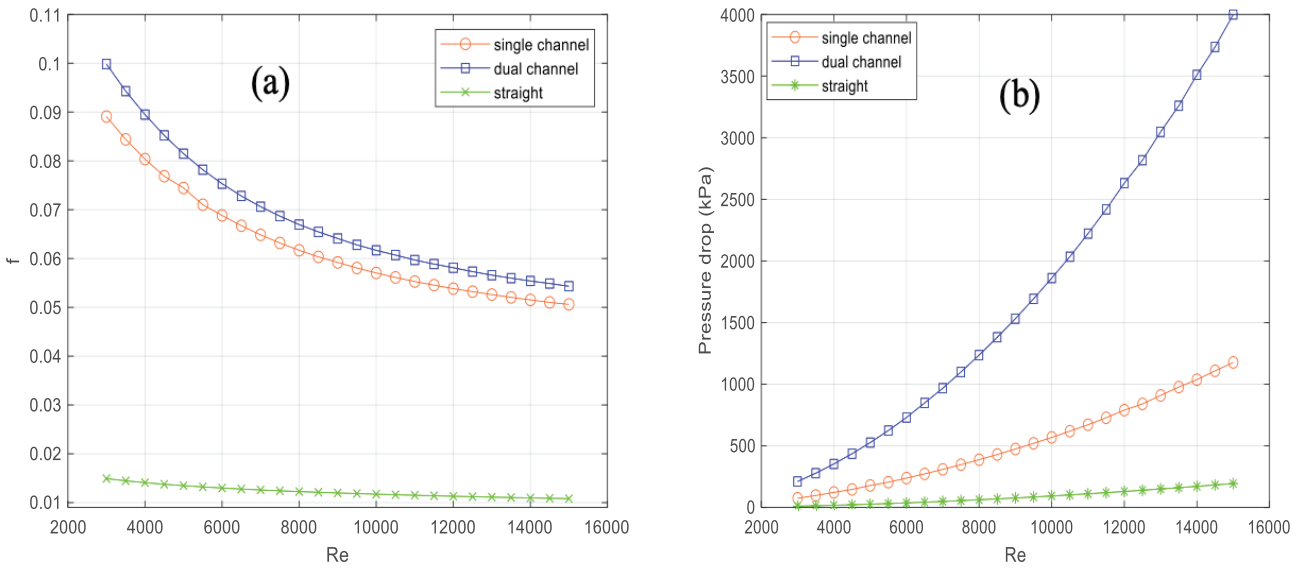


Figure 8. Variation of (a) friction factor and (b) pressure drop with Reynolds number for single, dual, and straight channels.

Average Flow Velocity Profile

In turbulent flow, the Nusselt number is highly dependent on the flow structure and average flow velocity profile. Figure 9 shows the influence of centrifugal force in the Archimedean spiral channel on the velocity profile. This additional force distorts the average velocity profile and moves the velocity peak toward the channel wall away from the center of the Archimedean spiral curve. It can be seen that the distortion in the velocity profile increases with the Reynolds number as the centrifugal force varies directly with the square of the average flow velocity. An interesting difference can be observed between the distorted velocity profiles of the dual and single spiral channels. In Single-channel (of 3 mm width), the velocity profile exhibits linear

variation near the channel centerline which is consistent with the behavior of the well-known turbulent velocity profile. This confirms that the turbulent flow can be developed within the single-channel. The effect of turbulence is, however, much less for the case of dual-channel (of 1.5 mm width) and the velocity profile is consistent with the distorted parabolic profile recently obtained [39].

Hydrothermal Performance

Figure 10 shows the hydrothermal performance of PEC of single and dual channels for different Reynolds numbers. It can be concluded that both single and dual channels have better PEC at a lower Reynolds number. The PEC of both channels drops exponentially with Reynolds number.

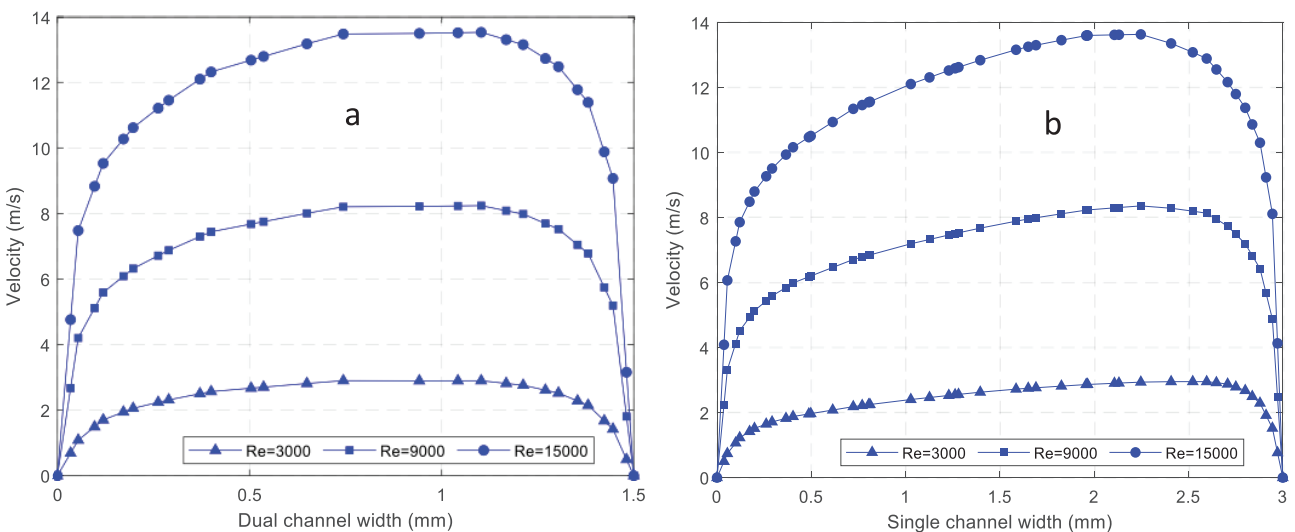


Figure 9. Velocity profile of (a) Dual and (b) Single channels.

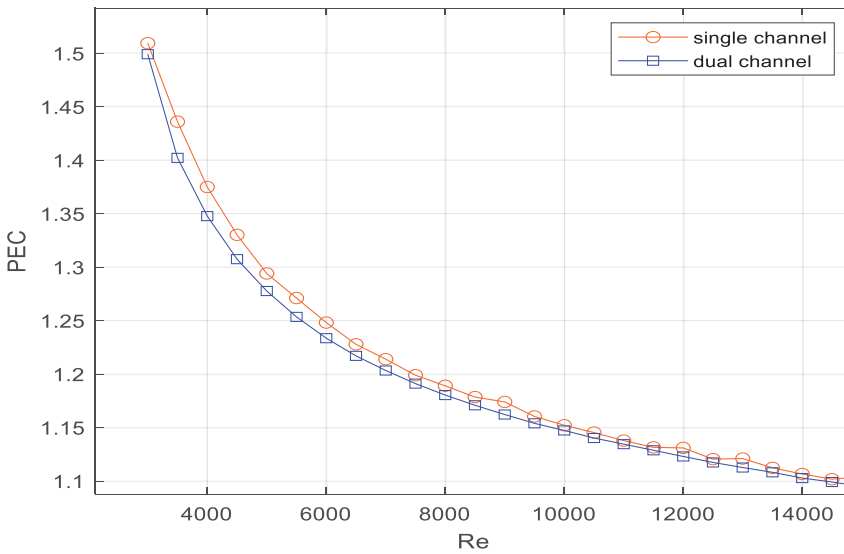


Figure 10. Variation of PEC with Reynolds number for single and dual channels.

At lower Re (3000-6000), the rate at which PEC drops is much higher for high Re (8000-15000). This is an important information to approach optimal PEC for specific channel configuration and flow conditions under specific CPU temperature limitations. The exponential drop in the PEC curve can be projected on the pressure drop as Reynolds number increases. It can be concluded from Figure 10 that the thermal cooling system should be working at a lower flow velocity for better hydrothermal performance.

CONCLUSION

The hydrothermal characteristics in the Archimedean spiral channel are studied numerically in this work. The heat sink model consists of a rectangular CPU (65 mm x 65 mm) attached to a circular cold plate of 105 mm diameter using an ethoxy layer of 0.2 mm thickness. The Archimedean spiral channel is grooved/drilled in the cold plate with two configurations; (1) a single channel of 3 mm X 5 mm cross-section area, and (2) dual channels of 1.5 mm X 5 mm. Water is used as a coolant with a range of inlet velocity such that Reynolds number varies from 3000 to 15000. The turbulent model used is Shear Stress Transport (k- ω) to offer better capturing of the flow with high viscous and fluctuation near-wall region. A constant heat flux of 106508.875 W/m² is applied on the bottom surface of the CPU. The external walls of the CPU, ethoxy, and cold plate are assumed to be adiabatic. The following conclusion can be drawn from this work:

- 1) The Archimedean spiral channels (single and dual) show good overall cooling performance and reduce the average CPU temperature below 46 °C for all Re values.
- 2) The channel configuration and Reynolds number have a decisive impact on CPU cooling and the average CPU

temperature decreases with Reynolds according to $T_{avg}^{single} = 45.96 + \frac{4793}{Re^{0.886}}$ and $T_{avg}^{dual} = 45.97 + \frac{8571}{Re^{0.980}}$ in °C for single and dual-channel, respectively.

- 3) No considerable difference was found between the average Nusselt number of the dual and single channels under the flow specification used in this work. However, relative to the straight channel, the Nusselt number increases by 52% for the dual spiral channel at Re=3000 and 55% at Re=15000. The correlations between the average Nusselt number with the Reynolds number were $Nu=0.0328 Re^{0.85} Pr^{0.4}$ for single-channel and $Nu=0.335 Re^{0.85} Pr^{0.4}$ for dual-channel with R² close to one.
- 4) Both single and dual channels have better hydrothermal performance (or PEC) at lower Reynolds numbers. The PEC of both channels drops exponentially with Reynolds number. At lower Re (3000-6000), the rate at which PEC drops is much higher for high Re (8000-15000).

NOMENCLATURE

<i>A</i>	Surface area, <i>m</i> ²
<i>C_p</i>	Specific heat, J/(Kg.K)
<i>C_f</i>	Skin friction factor
<i>D</i>	Diameter, <i>m</i>
<i>F₁</i>	First blinding function
<i>F₂</i>	Second blinding function
<i>f</i>	Fanning friction factor of single and dual channels
<i>H</i>	Height, <i>m</i>
<i>h_m</i>	Average heat transfer coefficient, W/(<i>m</i> ² .K)
<i>k</i>	Turbulent kinetic energy, J/kg
<i>k_f</i>	Thermal conductivity, W / (<i>m</i> .K)
<i>L</i>	Channel Length, <i>m</i>
<i>Nu</i>	Nusselt number

P	Pressure, Pa
Pr	prandtl number
q	heatflux, W/m^2
Q	Volume flowrate, m^3/s
Re	Reynolds number
R_{ij}	Reynolds stress tensor
T	Temperature, $^{\circ}C$
W	width, m

Greek symbols

ρ_f	Density of a fluid, kg/m^3
μ	Dynamic viscosity, $kg/(m.s)$
ν_t	Eddy viscosity, m^2/s
ϵ	Dissipation rate, m^2/s^3
δ_{wall}	Wall thickness, m
ω	Specific dissipation rate [1/s]

Subscripts

CPU	Refers to CPU
ch	Refers to channel
f	Refers to fluid
h	Refers to Hydraulic diameter of the channels
in	Refers to inlet
m	Refers to average
out	Refers to outlet
s	Refers to fluid-cold plate interface

AUTHORSHIP CONTRIBUTIONS

Authors equally contributed to this work.

DATA AVAILABILITY STATEMENT

The authors confirm that the data that supports the findings of this study are available within the article. Raw data that support the finding of this study are available from the corresponding author, upon reasonable request.

CONFLICT OF INTEREST

The author declared no potential conflicts of interest with respect to the research, authorship, and/or publication of this article.

ETHICS

There are no ethical issues with the publication of this manuscript.

REFERENCES

- [1] Zhang Z, Wang X, Yan Y. A review of the state-of-the-art in electronic cooling. *E-Prime* 2021;1:100009. [\[CrossRef\]](#)
- [2] Yang D, Yao Q, Jia M, Wang J, Zhang L, Xu Y, et al. Application analysis of efficient heat dissipation of electronic equipment based on flexible nanocomposites. *Energy Built Environ* 2021;2:157–166. [\[CrossRef\]](#)
- [3] Deng Y, Liu J. Design of practical liquid metal cooling device for heat dissipation of high performance CPUs. *J Electron Pack Trans ASME* 2010;132:1–6. [\[CrossRef\]](#)
- [4] Chan A, Wei J. Study on Alternative Cooling Methods Beyond Next Generation Microprocessors. ASME 2003 International Electronic Packaging Technical Conference and Exhibition, InterPACK 2003. [\[CrossRef\]](#)
- [5] Nada SA, El-Zoheiry RM, Elsharnoby M, Osman OS. Experimental investigation of hydrothermal characteristics of data center servers' liquid cooling system for different flow configurations and geometric conditions. *Case Stud Therm Eng* 2021;27. [\[CrossRef\]](#)
- [6] L.Boylestad R, Nashelsky L. *Electronic Devices and Circuit*. India: Pearson Education; 2014.
- [7] Mokrane M, Lounis M, Announ M, Ouali M, Djebiret MA, Bourouis M. Performance analysis of a micro heat exchanger in electronic cooling applications. *J Therm Eng* 2021;7:774–790. [\[CrossRef\]](#)
- [8] Zhang HY, Pinjala D, Teo PS. Thermal management of high power dissipation electronic packages: From air cooling to liquid cooling. *Proceedings of 5th Electronics Packaging Technology Conference, EPTC 2003:620–625*.
- [9] Tuckerman DB, Pease RFW. High-Performance Heat Sinking for VLSI. *IEEE Electron Device Letters* 1981;2:126–129. [\[CrossRef\]](#)
- [10] Chang JY, Park HS, Jo JI, Julia S. A system design of liquid cooling computer based on the micro cooling technology. *Thermomechanical Phenomena in Electronic Systems -Proceedings of the Intersociety Conference 2006;2006:157–160*.
- [11] Abdulnabi A, Sameer N, Mohammad H. Numerical and experimental investigation of heat transfer in liquid cooling serpentine mini-channel heat sink with different new configuration models. *Therm Sci Eng Progr* 2018;6:128–139. [\[CrossRef\]](#)
- [12] Sahu V, Joshi YK, Fedorov AG. Experimental investigation of hotspot removal using superlattice cooler. *2010 12th IEEE Intersociety Conference on Thermal and Thermomechanical Phenomena in Electronic Systems, ITherm 2010*. [\[CrossRef\]](#)
- [13] Mandel RK, Bae DG, Ohadi MM. Embedded two-phase cooling of high flux electronics via press-fit and bonded FEEDS coolers. *J Electron Pack Trans ASME* 2018;140:1–10. [\[CrossRef\]](#)
- [14] Sohel MR, Saidur R, Sabri MFM, Kamalisarvestani M, Elias MM, Ijam A. Investigating the heat transfer performance and thermophysical properties of nanofluids in a circular micro-channel. *Int Commun Heat Mass Transf* 2013;42:75–81. [\[CrossRef\]](#)
- [15] Taşkesen E, Tekir M, Pazarlıoğlu HK, Gurdal M, Gedik E, Arslan K. The effect of MHD flow on hydrothermal characteristics of ferro-nano-fluid in circular pipe. *Exp Heat Transf* 2022:1–15. [\[CrossRef\]](#)

- [16] Pazarlıoğlu HK, Gurdal M, Tekir M, Arslan K, Gedik E. Impact of twisted ducts with different twist ratios on heat transfer and fluid characteristics of nio/water nanofluid flow under magnetic field effect. *Heat Transf Res* 2022;53:55–71. [\[CrossRef\]](#)
- [17] Pazarlıoğlu HK, Tekir M. Impact of Fe₃O₄ / water on Natural Convection in Square Enclosure. *Eur J Sci Technol* 2021;28:675–683. [\[CrossRef\]](#)
- [18] Gaikwad VP, More SP. CPU Processor Cooling by using Microchannel Heat Sink with PCM as Coolant *Int J Eng Res Technol* 2017;6:214–219.
- [19] Algburi NİH, Pazarlıoğlu HK, Arslan K. Effect of pitch ratio and diagonal length of pin fin of heat sink on convective heat transfer for turbulent flow condition. *Eur J Sci Technol* 2021:643–652. [\[CrossRef\]](#)
- [20] Pazarlıoğlu HK, Ekiciler R, Arslan K. Numerical analysis of effect of impinging jet on cooling of solar air heater with longitudinal fins. *Heat Transf Res* 2021;52:47–61. [\[CrossRef\]](#)
- [21] Al-Tae'y KA, Jaddoa AA, Abd HS, Kadhim RA. A loop thermosyphon for liquid cooled minichannels heat sink with pulsate surface heat flux. *J Therm Eng* 2021;7:1030–1038. [\[CrossRef\]](#)
- [22] Ghani IA, Sidik NAC, Kamaruzaman N. Hydrothermal performance of microchannel heat sink: The effect of channel design. *Int J Heat Mass Transf* 2017;107:21–44. [\[CrossRef\]](#)
- [23] Al-Neama AFM. Serpentine minichannel liquid-cooled heat sinks for electronics cooling applications. [Doctorial Thesis]. The University of Leeds School of Mechanical Engineering Institute of ThermoFluids 2018:298.
- [24] Sharma A, Rajoria CS, Singh D, Bhamu JP, Kumar R. Numerical simulation of heat transfer characteristics of taper helical and spiral tube heat exchanger. *J Therm Eng* 2021;7:1591–1603. [\[CrossRef\]](#)
- [25] Jilte R, Ahmadi MH, Kumar R, Kalamkar V, Mosavi A. Cooling performance of a novel circulatory flow concentric multi-channel heat sink with nanofluids. *Nanomaterials* 2020;10:647. [\[CrossRef\]](#)
- [26] Umehara M, Yamada K, Rossman W. *Differential Geometry Of Curves And Surfaces*. World Scientific Publishing Company; 2017. [\[CrossRef\]](#)
- [27] Çengel YA, Ghajar AJ. *Heat and Mass Transfer: Fundamentals \& Applications*. New York: McGraw Hill Education; 2015.
- [28] Ozturk E. CFD analyses of heat sinks for cpu cooling with fluent. Madison: CWL Publishing Enterprises, Inc; 2004. p. 352. [\[CrossRef\]](#)
- [29] Alfonsi G. Reynolds-averaged Navier-Stokes equations for turbulence modeling. *Appl Mech Rev* 2009;62:1–20. [\[CrossRef\]](#)
- [30] Menter FR, Kuntz M, Langtry R. ten years of industrial experience with the SST turbulence model. *Heat Mass Transf* 2003:625–632.
- [31] Rocha PAC, Rocha HHB, Carneiro FOM, Vieira da Silva ME, Bueno AV. K- ω SST (shear stress transport) turbulence model calibration: A case study on a small scale horizontal axis wind turbine. *Energy* 2014;65:412–418. [\[CrossRef\]](#)
- [32] Elsaadawy E, Mortazavi H, Hamed MS. Turbulence modeling of forced convection heat transfer in two-dimensional ribbed channels. *J Electron Pack* 2008:130. [\[CrossRef\]](#)
- [33] Xu F, Lu H, Chen Z, Guan Z, Chen Y, Shen G, et al. Selection of a computational fluid dynamics (CFD) model and its application to greenhouse pad-fan cooling (PFC) systems. *J Clean Prod* 2021;302:127013. [\[CrossRef\]](#)
- [34] Khan MZU, Younis MY, Akram N, Akbar B, Rajput UA, Bhutta RA, et al. Investigation of heat transfer in wavy and dual wavy micro-channel heat sink using alumina nanoparticles. *Case Stud Therm Eng* 2021;28. [\[CrossRef\]](#)
- [35] Fan JF, Ding WK, Zhang JF, He YL, Tao WQ. A performance evaluation plot of enhanced heat transfer techniques oriented for energy-saving. *Int J Heat Mass Transf* 2009;52:33–44. [\[CrossRef\]](#)
- [36] Dittus FW, Boelter LMK. Heat transfer in automobile radiators of the tubular type. *Int Commun Heat Mass Transf* 1985;12:3–22. [\[CrossRef\]](#)
- [37] Liu J, Hussain S, Wang J, Wang L, Xie G, Sundén B. Heat transfer enhancement and turbulent flow in a high aspect ratio channel (4:1) with ribs of various truncation types and arrangements. *Int J Therm Sci* 2018;123:99–116. [\[CrossRef\]](#)
- [38] Das L, Rubbi F, Habib K, Saidur R, Islam N, Saha BB, et al. Hydrothermal performance improvement of an inserted double pipe heat exchanger with Ionanofluid. *Case Stud Therm Eng* 2021;28:101533. [\[CrossRef\]](#)
- [39] Chatterjee R, Duryodhan VS, Agrawal A. Impact of aspect ratio and thermophysical properties on heat transfer behavior in spiral microchannel. *Int J Therm Sci* 2022;172:107335. [\[CrossRef\]](#)